Revision 1

Impact of preparation method and chemical composition on physicochemical and photocatalytic properties of nano-dimensional magnetite-type materials

Zara P. Cherkezova-Zheleva[1]*, Katerina L. Zaharieva[1], Martin P. Tsvetkov[2], Vilma S. Petkova[3,4], Maria M. Milanova[2] and Ivan G. Mitov[1]

[1]*Institute of Catalysis, Bulgarian Academy of Sciences, "Acad. G. Bonchev" Str., Bl.11, 1113 Sofia, Bulgaria*

E-mail address: zzhel@ic.bas.bg

[2]*Faculty of Chemistry and Pharmacy, St. Kliment Ohridski University of Sofia, 1 J. Bourchier Blvd., 1164 Sofia, Bulgaria*

[3]*Institute of Mineralogy and Crystallography, Bulgarian Academy of Sciences, Acad. G. Bonchev Str., Bl. 107, 1113 Sofia, Bulgaria*

[4]*New Bulgarian University, Montevideo 21 Str., 1618 Sofia, Bulgaria*

Abstract

Nickel ferrites with different Ni content - $Ni_xFe_{3-x}O_4$, $0 \leq x \leq 1$ are technologically important materials for microwave, electronic and magnetic storage devices. They are members of solid solution series of spinel-type materials (Fe_3O_4 – $NiFe_2O_4$) having specific magnetic properties and different degree of electron delocalization. They demonstrate good gas sensing properties and catalytic activity in various catalytic processes, such as complete oxidation of waste gases, oxidative dehydrogenation of hydrocarbons, decomposition of alcohols etc. The preparation of such materials is still actual problem due to a number of difficulties in their synthesis and use of special techniques.

A series of nickel - containing ferrite materials $Ni_xFe_{3-x}O_4$ (x = 0.25, 0.5, 1) are prepared by precipitation method using $FeCl_3 \bullet 6H_2O$, $FeCl_2 \bullet 4H_2O$ and $NiCl_2 \bullet 6H_2O$ as precursors. The performed analyses show the dependence of the rate of formation of the spinel phase on the chemical composition. In order to obtain the exact conditions for a single-phase spinel material preparation a number of investigations have been performed: thermal analysis (thermogravimetry, differential thermogravimetry and differential thermal analysis) and various studies of the intermediates by powder X-ray diffraction, Mössbauer spectroscopy (at room and liquid nitrogen temperature), BET method and SEM. As a result, the appropriate conditions of obtaining monophase nanomaterials of doped magnetite are found. The synthesis involves a precipitation process combined with a low temperature heat treatment of materials (at 300°C and in argon atmosphere) or mechanochemical processing. Application of the second procedure leads to two interesting results: 1) synthesis of the target compounds under soft and clean conditions without heating, which is important for industrial technology and environmental protection and 2) the prepared samples have better characteristics (higher dispersion degree, better magnetic properties and higher activity in photocatalytic purification of wastewater from the textile industry).

Keywords: spinels, doped nano-sized magnetite, synthesis, mechanochemistry, relaxation phenomena, magnetic properties, photocatalytic activity

Introduction

The superparamagnetic nanometer scale composites, with its special properties, have been widely applied in the fields of electronic, chemical and machinery industries, aviation and spaceflight, energy production and metallurgy, environmental protection and medical treatment (Miani and Maurigh (2004), Wang (2003) and Balaz (2008)). Fe_3O_4 nanoparticles are one of several widely used magnetofluids. However, its saturation magnetization is generally insufficient to meet the requirements of their applications. Many research groups have proved that the magnetic performance of ferromagnetic nanoparticles, in particular Fe_3O_4, could be improved by doping them with transition metals or rare earth elements (Zhang et al. (2008); Wesselinowa and Apostolova (2007)). Magnetite and cation substituted magnetites are among of the extensively studied spinels. Nevertheless, certain aspects of their electronic and magnetic properties are still not fully understood. Further studies are needed to elucidate their behavior as sorbents, catalysts, pigments, etc. A virtually complete experimental data set for an interesting local quantity at impurities in the simple ferromagnets is thus now available. This leads to many attempts for a theoretical understanding. For the impurities in a lattice of metal iron a semiquantitative picture was developed that reproduced the experimental trend quite successfully (Stearns (1987) and Haas (2003)). The electrical conductivity mechanism of spinel ferrites containing Fe^{2+} ions is explained by the electron hopping effect between Fe^{2+} and Fe^{3+} ions in octahedral sites (Russo and Salahub (2000)). Cation distribution between tetrahedral (A) and octahedral (B) sites is a fundamental aspect on the understanding of their magnetic properties. Nickel-doped magnetite, $Ni_xFe_{3-x}O_4$, is an inverse spinel in which the Ni^{2+} ions are assumed to occupy preferentially B sites whereas Fe^{3+} are distributed between A and B sites. The degree of inversion (meaning the proportion of divalent cations occupying octahedral sites) of the doped-magnetite may vary, depending on the synthesis conditions (Lelisa et al, (2003)). The replacement of Fe^{2+} by Ni^{2+} does not change essentially the nature of crystallographic structure but shifts its unit cell dimension. The cation distribution in spinels has been a topic of interest as it affects their magnetic, electric and thermodynamic properties (Sawatzky et al. (1969); Russo and Salahub (2000)). In addition, it has been found that ferrite particles of similar composition differ on their magnetic properties depending on the preparation method. One reason for such a behavior is believed to be differences in particle size and shape. Decreasing the particle sizes leads to an increase of non-magnetic species on the particle surface (Sawatzky et al. (1969)). Various preparation procedures, including hydrothermal, co-precipitation, sol-gel methods and mechanical alloying have been used to produce ferrites (Lelisa et. al. (2003)). Some works have been reported on the formation of magnetite from mine drainage (Balaz P. (2008)) and from a combination of $Fe(OH)_2$ and $Fe(OH)_3$ (Schwertmann U. and Cornell R. (1991)). Many ore bodies such as nickel laterite and manganese nodule contain goethite having base metals like Cu, Ni or Co incorporated with the matrix (Schwertmann and Cornell (1991); Mohapatra (2005)). As the preparation of nanomaterials is sensitive to high temperature treatment at prolonged reaction time they should be avoided. In addition the use of high temperature often leads to problems with phase separation and nonstoichiometry. In this regard there is an increased interest in the development of new synthetic methods. For example, a direct mechanochemical route for preparation of spinel ferrites has been reported starting from metal oxide (MO) and α-Fe_2O_3 powder applied in equimolar ratio (Sepelak et. al. (1998)). However, in this method, the reactant is also the nonactivated α-Fe_2O_3/MO mixture, so it is difficult to achieve a single homogeneous spinel phase. Alternative wet chemical methods have been proposed, including co-precipitation from aqueous solution (Maaz et. al. (2009)), sol-gel synthesis involving supercritical drying to provide aerogels (Sivakumar (2011); Willey (1993)) and use of micellar microemulsions (Pileni (2001); Liu et. al. (2002)). In these cases, however, it is difficult to prevent contamination of the product by cations arising from the precipitants or organic residues from the precursor mixtures. To avoid compromising the purity and properties of spinel ferrite and related materials it would be desirable to prepare them from a single solid precursor in which the M^{2+} and Fe^{3+} cations are uniformly distributed on an atomic level. For this purpose layered double hydroxides (LDHs) can be used. LDHs are known as hydrotalcite-like materials also. They are a class of two-dimensional nanostructured anionic clays whose structure can be described as containing brucite-like layers in which a fraction of the divalent cations have been replaced isomorphously by trivalent cations giving positively charged sheets with change-balancing anions between the layers (Rives (2001)). LDHs have the general formula $[M^{2+}_{1-X}M^{3+}_{X}(OH)_2]^{X+}(A^{n-})_{X/n}\cdot mH_2O$, where M^{2+} and M^{3+} are di- and trivalent cations respectively, including Mg^{2+}, Fe^{2+}, Co^{2+}, Cu^{2+}, Ni^{2+}, or Zn^{2+} and Al^{3+}, Cr^{3+}, Ga^{3+}, Mn^{3+}, or Fe^{3+}, respectively; the value of the coefficient x is equal to the molar ratio of $M^{2+}/(M^{2+}+M^{3+})$; and A^{n-} is an anion, such as CO_3^{2-}, SO_4^{2-}, NO^{3-}, F^-, Cl^-, or PO_4^{3-} (Rives, V. (ed.) (2001)). Therefore, a large class of isostructural materials considered complementary to aluminosilicate clays with widely varied physicochemical properties can be obtained by changing the nature of metal cation, the molar ratio of M^{2+}/M^{3+}, and the type of the interlayer anion. These materials are potential precursors for preparation of spinel ferrites because they are often formed with mixtures of the same cations and have been shown to have an absence of long-range cation ordering. Calcination of LDHs at intermediate temperatures (450-600°C) affords formation of poorly crystalline mixed metal oxides. Calcination above 750°C is known to give spinels, but these are always mixed with the oxide of divalent metal (Fernandez et. al. (1998)). This reflects the fact that in LDHs, the divalent cations are always present in greater amount than the trivalent cations, whereas in a spinel the required molar ratio of M^{2+}/M^{3+} is 0.5. Preparation of high-quality magnetic nanoparticles with a narrow size distribution, reproducible physical properties and production within the short processing times is one of the key issues in nanoparticle research today.

The aim of presented paper is to obtain a single phase nano-sized nickel ferrites $Ni_xFe_{3-x}O_4$ (x=0.25, 0.5, 1) having good catalytic and magnetic properties. A series of nickel-doped magnetites were prepared by a combination of precursor co-precipitation and low-temperature heat treatment of materials (300°C and argon atmosphere) or mechanochemical processing. The structural properties of samples at each stage of the synthesis are studied in details, in an effort to identify some effects of the doping cations and preparation procedure on the magnetic, crystallographic, morphological and photocatalytic properties of the resulting spinel.

Experimental methods

Preparation of materials

The nickel ferrite materials with different stoichiometry: **Sample A** - $Ni_{0.25}Fe_{2.75}O_4$, **Sample B** - $Ni_{0.5}Fe_{2.5}O_4$ and **Sample C** - $NiFe_2O_4$ were synthesized by chemical co-precipitation method. The 0.03 M solutions of $FeCl_2$•$4H_2O$, $FeCl_3$•$6H_2O$, $NiCl_2$•$6H_2O$ (Sigma-Aldrich, 99.99%) were prepared with distilled water and mixed in a ratio of

3:8:1, 1:4:1, 0:2:1. As precipitating agent 0.3 M NaOH (Sigma-Aldrich, pellets, ≥ 97%) was added slowly by drops at continuous stirring until pH value became 12.5. This pH value has been experimentally obtained. It should provide the appropriate conditions for co-precipitation of studied compounds. After co-precipitation procedure the mixture was stirred for one hour. The prepared brown precipitates were centrifuged and washed several times with distilled water up to pH=7. The product was dried at 50°C for 3 h. In order to prepare single phase spinel materials the co-precipitated samples were mechanochemically treated using stainless steel container with volume 250 ml. The mass ratio between sample and balls is 1:30. The milling activation process is carried out in high energy planetary ball mill type PM 100, Retsch, Germany. The **Sample D** was prepared after mechanochemical treatment of **Sample B** for 3 hours in nitrogen media and rotation speed 500 rpm (Cherkezova-Zheleva et. al. (2013)). **Sample E** was obtained by thermal treatment of **Sample B** at 300 °C in argon atmosphere for 3 hours.

Physicochemical methods for characterization of nickel ferrite materials

The phase composition and magnetic properties of the prepared nickel ferrite samples were tested by powder X-ray diffraction, Mössbauer and thermal analyses, BET method and SEM.

X-ray diffraction (XRD) analysis of the produced powder ferrite materials was performed by a TUR M62 apparatus with PC management and data accumulation using HZG-4 goniometer and CoKα radiation. JCPDS database (Powder Diffraction Files, Joint Committee on Powder Diffraction Standards, Philadelphia PA, USA, 1997) was used for the phase identification. Scherrer equation was used to made calculation of the average crystallite size, lattice microstrain parameter and unit cell parameter of the ferrite samples (Schwertmann and Cornell (1991)).

Mössbauer spectra at room temperature (RT) and liquid nitrogen temperature (LNT) were recorded using apparatus Wissenschaftliche Elektronik GmbH, working with a constant acceleration mode, ^{57}Co/Cr source, α-Fe standard. The computer fitting was used to determine the parameters of hyperfine interactions of Mössbauer spectral components: isomer shift (IS), quadrupole splitting (QS), hyperfine effective magnetic field in the site of iron nuclei (H_{eff}), line widths (FW) and component relative weights (G). Values of errors are on the order of ±0.01 mm/s for the IS, ±0.02 mm/s for the QS, ±2T for H_{eff}, 0.4 mm/s for FWHM and ±2% for G, respectively.

Nitrogen adsorption–desorption isotherms were determined on Sorptomatic 1990 Thermo Finnigan automatic system using nitrogen physisorption at −196°C. Before measurement the samples were outgassed at 100°C for 10 h. Specific surface area of the samples (S_{BET}) was calculated from the nitrogen adsorption isotherms according to the Brunauer, Emmett, and Teller method (Rouquerol et. al. (1999)). The micropores were analyzed using Dubinin–Radushkevich method (Dubinin (1975)). Pore size, pore volume distribution, bulk density and porosity were determined by mercury intrusion porosimetry (Carlo Erba 2000 porosimeter with Macropores unit 120).

Surface microstructure of the films was visualized under scanning electron microscope Philips SEM 515, the samples preparation being described in details earlier (Starbov et. al. (2007)).

The thermal analysis (TG, DTG and DTA) were performed with a Stanton Redcroft (Great Britain) installation equipped with a PC. The produced ferrite materials (10.00

mg) were thermally treated in the temperature range 20–1000°C at 10°C/min heating rate in stabilized corundum crucible and air media with flow rate of 1l/h.

Results and discussion

Series of nickel contained ferrite samples with respective stoichiometry for $Ni_xFe_{3-x}O_4$ (x=0.25, 0.5 and 1) were produced using co-precipitation procedure. The expected phase composition of these materials is related to formation of green rusts having LDH-type structure and different degree of incorporation of Ni metal ion in the host matrix is expected. Physicochemical characterization of prepared precursor materials was done by recording their Mössbauer spectra and XRD patterns. Figures 1 and 2 show the respective results.

In all three cases the Mössbauer spectra represent superposition of doublet-type lines only. The spectra are fitted by the CONFITA program using several models for the fitting procedures. The best spectra fit show the presence of two doublet components in all registered spectra. The calculated values of hyperfine parameters, the relative weights and FWHM after spectra evaluation are listed in Table 1. The determined hyperfine parameters of the two sets of doublet lines (Dbl. 1 and Dbl. 2) can be assigned to preparation of ultradisperse iron oxide particles (D < 10 nm) and to a presence of Ni-Fe-LDH and/or akagenaite phase (β-FeOOH) phase. For the ultradisperse iron oxide (magnetite-type) particles is characteristic so-called superparamagnetic (SPM) behaviour due to thermally activated reversals of the particles magnetization (Dumesic and Topsoe (1977); Van Der Kraan (1973); Niemantsverdriet et. al. (1985); Musić et. al. (2004)). The resulting effect of SPM case is the absence of magnetic hyperfine structure in the Mössbauer spectra. Then the core-shell model (Van Der Kraan (1973);

Niemantsverdriet et. al. (1985)) can be applied to explain these two quadrupole doublets. They belong to iron ions from the "core" and the interface ("shell layers") of the nanoparticles. The doublet (Dbl. 1) with lowest QS value belongs to iron ions from the "core" of the particles. The doublet (Dbl. 2) with larger QS value can be assigned to interface (from the "shell" layers) ferric ions. The lower symmetry in the environment of the "surface" iron ions results in a change in the electric field gradient and therefore in a shift of the QS. Because of the very close parameters of SPM spinel particles and LDHs phase in Mössbauer spectra the exact phase composition cannot be determined. Partial resolution of the spectra and verification was done by registration of LNT Mössbauer spectra of precursors. Figure 3 and Table 1 show one of them for example.

The X-ray diffraction analysis of starting co-precipitated precursors (Fig. 2) shows the presence of low-intensity and broad patterns, halo-peaks and X-ray amorphous background. It was established the presence of non-stoichiometric spinel phase $Ni_xFe_{3-x}O_4$ (PDF-10-0325; PDF-75-0449) and additional phases β-FeOOH (PDF-75-1594) and iron-nickel hydrotalcite phase (PDF-14-0191). So the spinel synthesis starts on the precipitation process. Additional nickel-contained phases are not registered.

In order to prepare single phase materials number of thermal analyses are carried out. The behaviour of synthesized ferrite materials during the thermal treatment gives results concerning the further investigations about effect of calcinations as the dehydration and dehydrogenation temperatures and crystallisation processes (see Fig. 4). On the base of the obtained results, thermal behavior of investigated materials is resolved. Three stages of weight loss in the TG curves are established. The main mass losses - 8.6%, 16.7% and 15.7% results from dehydration process. The presence of endothermic peak in the temperature region 20-200°C is related to removal of water molecules coordinated in crystal lattice. The exothermic effects at 348.0°C, 356.8°C of the ferrite materials **Sample A** - $Ni_{0.25}Fe_{2.75}O_4$ and **Sample B** - $Ni_{0.5}Fe_{2.5}O_4$ in the DTA curves and weight losses 7.8%, 5.1% and 6.5% are assigned to the thermal transformation of intermediate phases (β-FeOOH and LDHs) (Schwertmann and Cornell (1991)). A high presence of hematite due to a low content of nickel in spinel ferrite $Ni_{0.25}Fe_{2.75}O_4$ explains the more intensive exothermic peak at 348.0°C compared with this one at 356.8°C for $Ni_{0.5}Fe_{2.5}O_4$. The absence of exothermic effect around this temperature in the thermal behavior of ferrite material **Sample C** - $NiFe_2O_4$ is connected with the presence of single spinel ferrite phase only. The registered DTA thermograms of all studied samples show the second exothermic peak at 590.7°C, 565.0°C and 554.6°C, respectively. It can be attributed to complete formation and crystallization of spinel ferrite phase in all prepared samples.

These results are confirmed by study of samples after thermal analysis. Mössbauer spectra of **Samples A, B** and **C** after thermal treatment are presented on Figure 5 (suppl.). In all cases the spectra represent superposition of sextet-type lines only. The best spectra fit show the presence of two or three sextet components in all registered cases. The calculated Mössbauer parameters are shown in Table 1. The obtained hyperfine parameter values of these components show presence of tetrahedrally coordinated Fe^{3+} ions in a spinel phase (Sxt1) and octahedrally coordinated Fe^{3+} ions in a spinel phase (Sxt2). The calculated hyperfine parameter values of the third sextet component (Sxt 3) show the presence of octahedrally coordinated iron ions in third oxidation degree, which are included in the α-Fe_2O_3 (Hematite) phase (Schwertmann and Cornell (1991)). With an increase of Ni content, the relative weight of hematite phase decreases and in the case of **Sample C** only octahedrally and tetrahedrally coordinated iron ions in spinel structure are detected (Schwertmann and Cornell (1991)).

Figure 6 shows the XRD patterns of nickel contained ferrite materials after thermal analysis. The formation of the non-stoichiometric spinel ferrite phase $Ni_xFe_{3-x}O_4$ (PDF-10-0325; PDF-75-0449) and different amount of hematite α-Fe_2O_3 phase (PDF-73-2234) are observed in the **Sample A -** $Ni_{0.25}Fe_{2.75}O_4$ and **Sample B -** $Ni_{0.5}Fe_{2.5}O_4$ respectively. Diffraction peaks due to single phase cubic spinel ferrite $NiFe_2O_4$ (PDF-10-0325) are indexed in the **Sample C -** $NiFe_2O_4$. The registered sharp lines in all three XRD patterns indicate the presence of relatively well crystallized ferrite materials.

In order to prepare single phase materials the co-precipitated samples were heated in an inert atmosphere to avoid oxidation. The interpretation of the above presented thermal analysis data gives as a result the appropriate temperature of heating to be 300°C. The crystal water from the materials is dehydrated at temperatures lower than 300°C and therefore this is the lowest temperature to start the synthesis in isothermal conditions. A fresh reaction surface is formed during the process of dehydration. Getting a fresh reactive surface and the heating in the inert atmosphere provide the appropriate conditions for the synthesis of spinel compounds. Figure 7-a presents the X-ray diffraction pattern of **Sample E -** $Ni_{0.5}Fe_{2.5}O_4$ after heating at 300°C in inert atmosphere (Ar media) as an example. It clearly shows the preparation of ultra-dispersed single phase spinel material. The exact composition of sample will be established by chemical analysis, but all studied materials are members of solid solution series Fe_3O_4 (PDF-75-0449) – $NiFe_2O_4$ (PDF-10-0325). The presence of single phase composition shows the incorporation of Ni^{2+} ions in the magnetite host matrix. Mössbauer spectrum of **Sample**

E - thermally synthesized nanosized ferrite material $Ni_{0.5}Fe_{2.5}O_4$ at RT and LNT, as well as the calculated relative hyperfine parameters completely confirmed this result (see Fig. 7-b and Table 1).

Mechanochemical activation of the initial precursors was studied (Cherkezova-Zheleva et. al. (2013)). The treatment of **Samples A, B** and **C** for 3 hours in nitrogen media and rotation speed 500 rpm lead to formation of single non-stoichiometric spinel nanosized nickel ferrite material. On Fig. 8-a XRD pattern of **Sample D** is presented. It can be seen the presence of spinel phase only - $Ni_{0.5}Fe_{2.5}O_4$ (PDF-10-0325; PDF-75-0449). X-ray amorphous halo peaks are also obtained. Registered broad and low-intensity diffraction peaks confirm the higher dispersion of mechanochemically prepared sample in comparison with thermally synthesized ferrite spinel **Sample E**. The average particle size, lattice microstrain parameter and unit cell parameter of studied spinel phase was calculated by Scherrer equation and Williamson-Hall diagram (Schwertmann and Cornell (1991); Williamson and Hall (1953)). The obtained values are: mean crystallite size of spinel particles is about 8nm for **Sample D** and about 11 nm for **Sample E.** The obtained results for the presented phases and their particle size are in very good agreement with presented Mössbauer data. Comparison of RT Mössbauer spectra of thermally and mechanochemically treated samples (see Fig. 7-b and 8-b) reveals the different dispersity of the samples. It is well seen that the thermal treatment of precursor gives the synthesis of single phase spinel material having both doublet and sextet type components. In the case of mechanochemically prepared sample Mössbauer spectrum includes only superparamagnetic doublet components. The calculated hyperfine parameters according core-shell model show the presence of 3-5nm spinel material in the second case and about 12nm in the thermally treated sample. This is confirmed by

LNT spectra of materials which calculated hyperfine parameters of spectra components are shown in Table 1.

As a result nanosized ferrite materials $Ni_{0.5}Fe_{2.5}O_4$ are prepared by two different synthesis routes: co-precipitation and low temperature or mechanochemical treatment of co-precipitated ferrite precursors. Study of magnetic properties of as-prepared materials shows superparamagnetic behavior of all precursor materials at room temperature and at liquid nitrogen temperature also. The mechanochemical activation and low thermal treatment at 300°C lead to formation of single spinel phase. Mechanochemical synthesis provides the possibility to prepare nanosized materials with enhanced magnetic properties in comparison with thermally treated one. These samples show higher dispersity which is of great importance to their catalytic properties.

The performed experimental studies about textural characteristics of prepared ferrite samples reveal the differences in the specific surface areas, maximum pore diameters and pore volumes of **Samples D** and **E** are affected by different routes for their production. Mechanochemically synthesized sample (S_{BET} = 168m^2/g; maximum pore diameter=3.5nm; pore volume=0.129cm^3/g) have better dispersity than thermally treated material (S_{BET} = 124m^2/g; maximum pore diameter=8.6nm; pore volume=0.339cm^3/g).

The morphology of the particles of **Samples D** and **E**, as they are visualized by SEM, are shown on Fig. 9. It is verified that the magnetite is doped with nickel and it tends to form uniform agglomerates of very small particles. Comparison of Fig. 9-a and 9-d clearly shows higher dispersion of mechanochemically prepared sample.

The results obtained by photocatalytic degradation of Malachite green oxalate dye under UV light using synthesized nickel ferrite materials as photocatalysts are presented on a

Figure 10 and in Table 2. The synthesized samples show good sorption abilities of the dye after the dark period varying between 69 and 79%. The sample preparation by mechanochemical activation leads to highest sorption properties for **Sample D** - $Ni_{0.5}Fe_{2.5}O_4$ (79%) than the other nickel ferrite samples. The increasing concentration of nickel ions in magnetite-type structure leads to higher apparent rate constant as **Sample A** - $Ni_{0.25}Fe_{2.75}O_4$ (8.7 x10^{-3} min^{-1}) < **Sample C** - $NiFe_2O_4$ (13.5 x10^{-3} min^{-1}). The co-precipitated **Sample C** - $NiFe_2O_4$ (13.5 x10^{-3} min^{-1}) possess the higher photocatalytic activity than that of the standard photocatalyst Degussa P25 (12x10^{-3} min^{-1}) determined in our laboratory under the same conditions. In conclusion the obtained nickel ferrite materials could be used as absorbents and photocatalysts for purification of dyes from waste water solutions.

Implications

Finding of new ways for preparation of nano-sized spinel ferrites is of great importance for synthesis of magnetic materials, electronics, catalysts, gas detectors, etc. The problem still exists due to a number of technological difficulties in their synthesis and use of special techniques. A series of nickel containing ferrite materials $Ni_xFe_{3-x}O_4$ (x= 0.25, 0.5, 1) are prepared by precursor precipitation as a first step. It was established the dependence of the rate of formation of the spinel phase of the chemical composition. The appropriate conditions of obtaining single-phase spinel nanosized materials of doped magnetite are found. The synthesis involves a precipitation process combined with a low temperature heat treatment in argon media at 300°C or mechanochemical processing of materials. Application of the second preparation procedure leads to two interesting results. Firstly mechanochemical treatment leads to synthesis of the target compounds under soft and ecologically friendly conditions without heating, which is important for industrial technology and environmental protection. Secondly the prepared samples have better characteristics as higher dispersion, better magnetic properties and higher photocatalytic activity in photocatalytic purification of wastewater from the textile industry. This method has the advantages of simple preparation, cost effective and gentle chemistry route resulting in ultrafine and homogeneous powder. The ability to obtain single-phase nickel ferrite magnetic nanoparticles with controllable particle size and size distribution improves its adequacy in a wide range of technological applications. As far as the magnetic properties of these materials are concerned, spin glass like behavior can be considered as the most interesting property that leads to high field irreversibility, shift of the hysteresis loops and anomalous relaxation dynamics which is an object of another investigation of authors (unpublished manuscript).

Acknowledgements

The financial support by the European Social Fund within the framework of Operating Program "Development of Human Resources" – **BG051PO001-3.3.05-0001** "Science and business" is gratefully acknowledged.

References cited

Balaz P. (2008) Mechanochemistry in Nanoscience and Minerals Engineering, Springer-Verlag, Berlin Heidelberg.

Cherkezova-Zheleva Z., Zaharieva K., Kunev B., Mitov I., Krstić J., (2013) Impact of mechanochemistry in ferrite catalyst preparation, Tribological Journal BULTRIB, III 203-207.

Dubinin M. (1975) Progress in Surface and Membrane Science, vol. 9, Academic Press, New York, NY.

Dumesic J., and Topsoe H. (1977) Mössbauer Spectroscopy Applications to Heterogeneous Catalysis. Advances in Catalysis, 26, 121-246.

Fernandez, J. M., Ulibarri, M. A., Labajos, F. M., and Rives, V. (1998) The effect of iron on the crystalline phases formed upon thermal decomposition of Mg-Al-Fe hydrotalcites. Journal of Materials Chemistry, 8, 2507-2514.

Haas H. (2003) Magnetic Hyperfine Fields at sp-Impurities in Cobalt and Nickel, Hyperfine Interactions, 15111, 52, 173-189.

Lelisa M. F. F., Fabrisa J. D., Mussela W. da Nova, and Takeuchi A. Y. (2003) Preparation and Characterization of Nickel- and Cobalt-doped Magnetites, Materials Research, Vol. 6, No. 2, 145-150.

Liu, C., Rondinone, A. J., and Wang, Z. (2002) Synthesis of magnetic spinel ferrite $CoFe_2O_4$ nanoparticles from ferric salt and characterization of the sized-dependent superparamagnetic properties, Journal of Pure and Applied Chemsitry, 72, 37-45.

Maaz K., Karim S., Mumtaz A., Hasanain S.K., Liu J., and Duan J.L. (2009) Synthesis and magnetic characterization of nickel ferrite nanoparticles prepared by co-precipitation route, Journal of Magnetism and Magnetic Materials 321, 1838–1842.

Miani F. and Maurigh F. (2004) Encyclopaedia of Nanoscience and Nanotechnology, Marcel Dekker, New York, pp. 1787–1795.

Mohapatra M., Pandey Brajesh, Upadhyay Chandan, Anand S., Das R.P., and Verma H.C., (2005) Effect of Ni doping on the properties of fine magnetite particles, Journal of Magnetism and Magnetic Materials, 295, 44–50.

Musić S., Krehula S., and Popović S., (2004) Thermal decomposition of β-FeOOH, Materials Letters, 58, 444-448.

Niemantsverdriet J. W., Van der Kraan A. M., Delgass W. N., and Vannice M. A. (1985) Small-particle effects in Mössbauer spectra of a carbon-supported iron catalyst. Journal of Physical Chemistry, 89, 67–72.

Pileni M. P. (2001) Magnetic Fluids: Fabrication, Magnetic Properties, and Organization of Nanocrystals, Advanced Functional Materials, 11, 323-336.

Rives, V. (ed.) (2001) Layered Double Hydroxides: Present and Future, Nova Science Publishers, New York.

Rouquerol, F., Rouquerol, J., Sing K. (1999) Adsorption by Powders and Porous Solids, Academic Press, London.

Russo N. and Salahub D. (Ed.) (2000) Metal-Ligand Interactions in Chemistry, Physics and Biology, NATO Sci. Series, Miesto, vol. 546.

Sawatzky, G.A, Van Der Woude, F., and Morrish, A.H. (1969) Mössbauer study of several ferromagnetic spinels, Physical Review, 187, 747-757.

Schwertmann U. and Cornell R. (1991) Iron Oxides in the Laboratory, Weinheim, New York-Basel-Cambridge.

Sepelak, V., Steinike, U., Uecker, D. Chr., Wissmann, S., and Becker, K. D. (1998) Structural Disorder in Mechanosynthesized Zinc Ferrite, Journal of Solid State Chemistry, 135, 52-58.

Sivakumar P., Ramesh R. , Ramanand A. , Ponnusamy S., and Muthamizhchelvan C. (2011) Preparation and properties of nickel ferrite ($NiFe_2O_4$) nanoparticles via sol–gel auto-combustion method, Materials Research Bulletin, 46, 2204–2207.

Starbov N., Krumov E., Kjosev B., Rachkova A., and Starbova K. (2007) Thermal post-processing of spray-pyrolysis deposited ZnO thin films, Journal of Optoelectronics and Advanced Materials, 9, 245-247.

Stearns, M. (1987). In Magnetic Properties of 3d, 4d and 5d Elements, Alloys and Compounds, K.-H. Hellwege and O. Madelung (Eds.), Landolt Börnstein, New Series III, Vol. 19a, Springer, Berlin.

Van Der Kraan A. (1973) Mössbauer effect studies of surface ions of ultrafine α-Fe_2O_3 particles, Physica Status Solidi A, 18, 215-226.

Wang G.-W. (2003) in Encyclopaedia of Nanoscience and Nanotechnology, Marcel Dekker, New York, pp. 1–9.

Wesselinowa J. M., and Apostolova I. (2007) Size, anisotropy and doping effects on the coercive field of ferromagnetic nanoparticles, Journal of Physics: Condensed Matter, 19, 406235.

Willey R. J., Oliver, S. A., Oliveri, G., and Busca, G. (1993) Chemistry and structure of mixed magnesium ferric oxide aerogels, Journal of Materials Research, 8, 1418-1427.

Williamson G.K., and Hall W.H. (1953) X-ray line broadening from filed aluminium and wólfram, Acta Metallurgica, 1, 22-31.

Zhang P. P., Han C. H., Cheng J. P., Chen X. G., Ye Y. (2008) Effect of La Doping on Magnetic Properties of Ferrite Prepared from Ocean Manganese Nodules, Chinese Journal of Inorganic Chemistry, 24, 307-310.

Figure captions

Figure 1. Mössbauer spectra of precursor materials.

Figure 2. XRD patterns of precursor materials.

Figure 3. Mössbauer spectrum of co-precipitated precursor material at LNT.

Figure 4. TG, DTG and DTA curves of synthesized nickel contained ferrite samples.

Figure 5 (suppl.). Mössbauer spectra of **Samples A, B** and **C** after thermal analysis.

Figure 6. XRD spectra of **Samples A, B** and **C** after thermal analysis.

Figure 7. Sample E (thermally synthesized $Ni_{0.5}Fe_{2.5}O_4$):

a.) XRD pattern; **b.)** Mössbauer spectrum at RT.

Figure 8. Sample D (mechanochemically synthesized $Ni_{0.5}Fe_{2.5}O_4$):

a.) XRD pattern; **b.)** Mössbauer spectrum at RT.

Figure 9- a). SEM image of **Sample D** at magnification 5000x.

b). SEM image of **Sample D** at magnification 10000x.

c). SEM image of **Sample E** at magnification 2000x.

d). SEM image of **Sample E** at magnification 5000x.

Figure 10. Concentration changes of Malachite green oxalate dye under UV irradiation time using nickel ferrite materials with different stoichiometry.

Table 1. Mössbauer parameters of samples

Sample	Components	IS, mm/s	QS, mm/s	H_{eff}, kOe	FMHW, mm/s	G, %
Sample A at RT	Dbl 1	0.36	0.53	-	0.36	53
	Dbl 2	0.36	0.92	-	0.43	47
Sample A at LNT	Sxt 1	0.52	-0.15	42.4	0.74	12.5
	Sxt 2	0.47	-0.04	44.8	0.38	4.9
	Sxt 3	0.82	-0.41	17.2	1.70	28.3
	Sxt 4	0.34	0.01	38.1	1.21	2.4
	Dbl 1	0.41	0.77	-	0.46	6.7
	Dbl 2	0.40	1.32	-	1.20	45.1
Sample B at RT	Dbl 1	0.36	0.55	-	0.34	52
	Dbl 2	0.37	0.93	-	0.38	48
Sample B at LNT	Sxt 1	0.56	-0.15	42.8	0.47	11.7
	Sxt 2	0.46	-0.05	44.8	0.44	23.0
	Sxt 3	0.80	-0.39	38.5	1.12	12.7
	Sxt 4	0.34	0.01	41.1	0.98	17.3
	Dbl 1	0.43	0.58	-	0.21	2.0
	Dbl 2	0.44	0.85	-	0.55	33.3
Sample C at RT	Dbl 1	0.36	0.54	-	0.33	63
	Dbl 2	0.36	0.90	-	0.35	37
Sample C at LNT	Sxt 1	0.52	-0.14	43.3	0.62	15.3
	Sxt 2	0.47	-0.05	39.8	0.92	23.2
	Sxt 3	0.34	0.01	28.1	1.57	16.7
	Dbl 1	0.45	0.48	-	0.36	17.3
	Dbl 2	0.45	0.86	-	0.62	27.4
Sample D at RT	Dbl 1	0.34	0.59	-	0.46	56.4
	Dbl 2	0.33	0.91	-	0.51	43.6
Sample D at LNT	Sxt 1	0.46	-0.05	43.4	0.84	20.0
	Sxt 2	0.81	-0.39	37.3	1.12	9.4
	Sxt 3	0.34	0.01	35.2	0.98	46.8
	Dbl 1	0.45	1.58	-	1.66	23.6
Sample E at RT	Sxt 1	0.34	0	41.1	1.52	15.9
	Sxt 2	0.35	0.01	10.3	2.27	38.3
	Dbl 1	0.34	0.62	-	0.41	7.6
	Dbl 2	0.33	0.93	-	0.87	38.1
Sample E at LNT	Sxt 1	0.48	-0.05	51.2	0.74	22.7

	Sxt 2	0.63	-0.32	49.2	0.62	18.5
	Sxt 3	0.36	0.02	48.1	0.98	58.8
Sample A - after TA	Sxt 1	0.34	-0.03	48.2	0.47	20
	Sxt 2	0.20	-0.02	51.6	0.32	17
	Sxt 3	0.37	-0.20	51.4	0.28	63
Sample B - after TA	Sxt 1	0.37	-0.01	48.5	0.41	35
	Sxt 2	0.26	-0.01	51.8	0.47	33
	Sxt 3	0.37	-0.19	51.3	0.28	32
Sample C - after TA	Sxt 1	0.37	0	48.7	0.37	49
	Sxt 2	0.25	0.01	52.2	0.43	51

Table 2. Apparent rate constants and sorption ability of nickel ferrite type materials

Sample	K_{app} (x10^{-3} min^{-1})	Sorption (%)
Sample A - $Ni_{0.25}Fe_{2.75}O_4$	8.7	77
Sample B - $Ni_{0.5}Fe_{2.5}O_4$	6	69
Sample C - $NiFe_2O_4$	13.5	75
Sample D - $Ni_{0.5}Fe_{2.5}O_4$ - MCS	9.4	79
Sample E - $Ni_{0.5}Fe_{2.5}O_4$ - TS	9.3	74

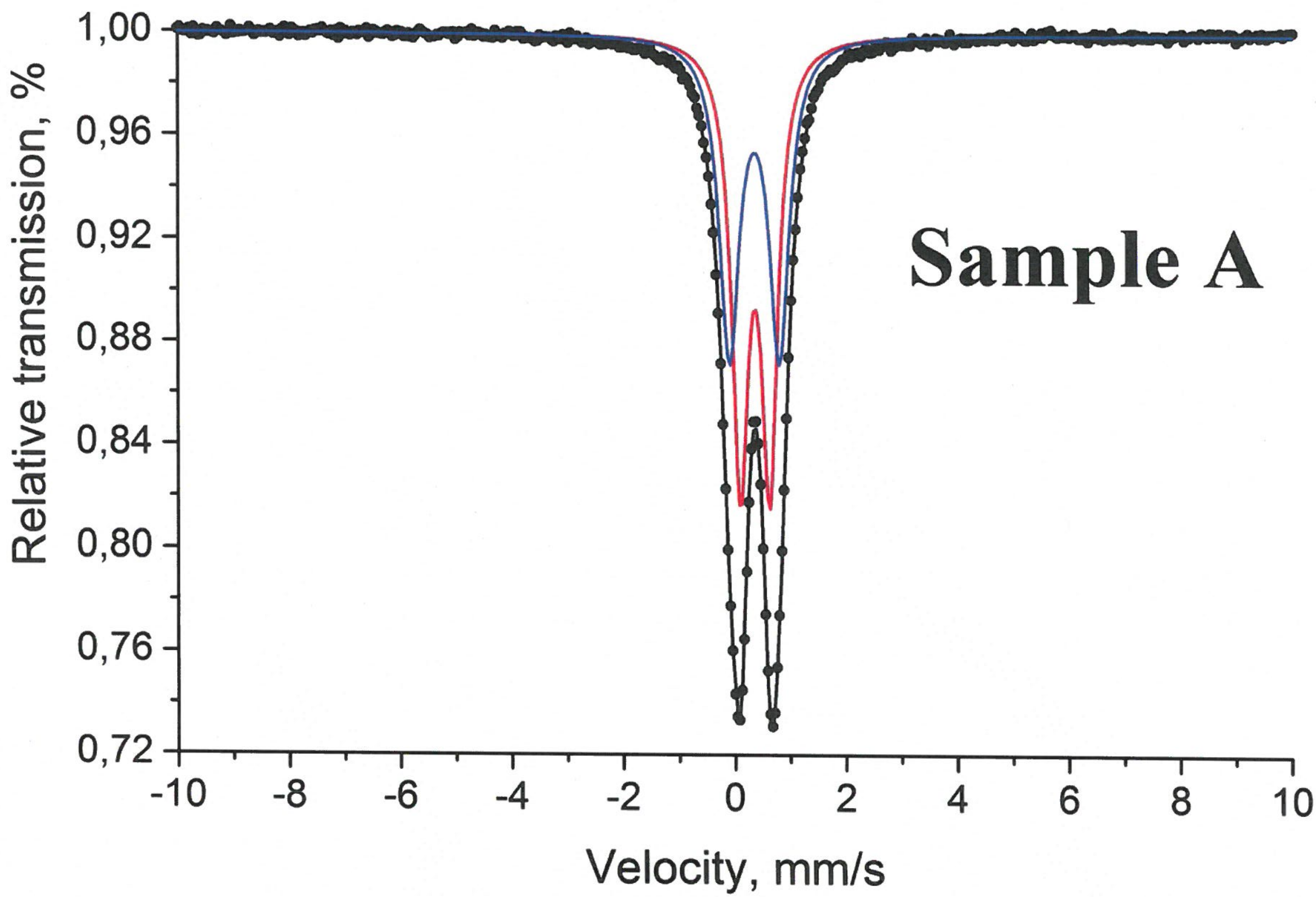
Sample A
1,00
0,96
0,92
0,88
0,84
0,80
0,76
0,72
Relative transmission, %
-10
-8
-6
-4
-2
0
2
4
6
8
10
Velocity, mm/s

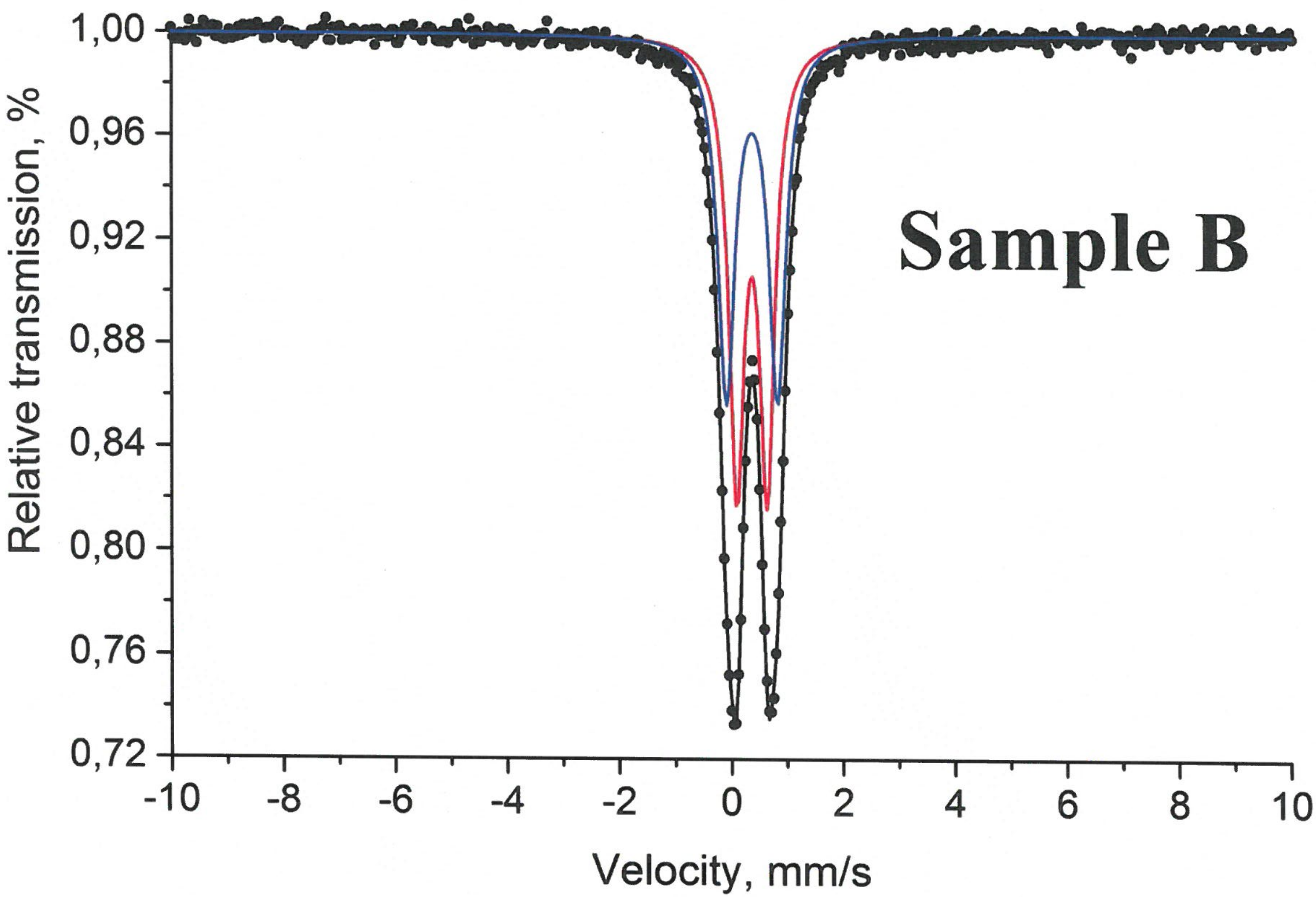
Sample B
Relative transmission, %
1,00
0,96
0,92
0,88
0,84
0,80
0,76
0,72
-10
-8
-6
-4
-2
0
2
4
6
8
10
Velocity, mm/s

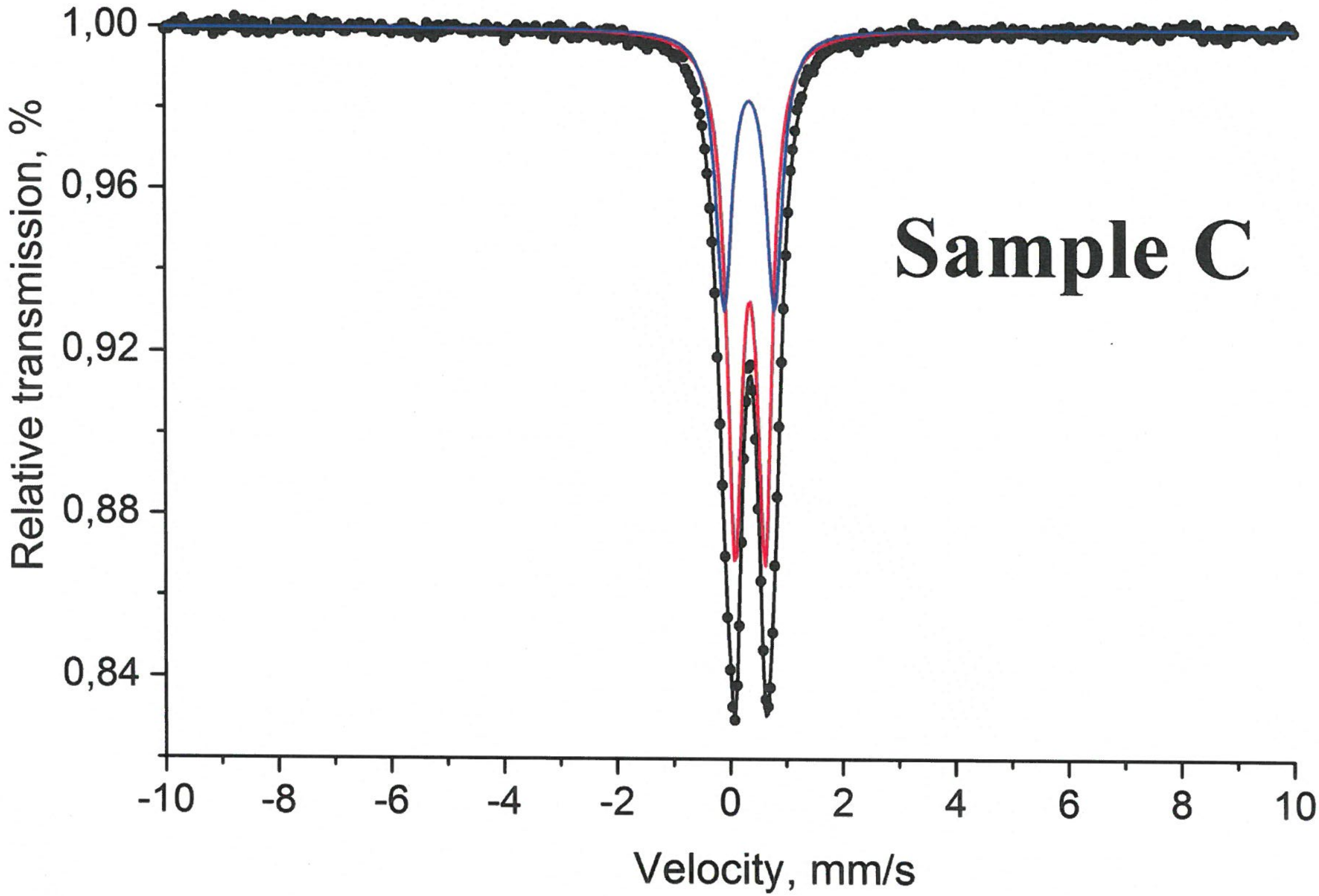
Sample C
Relative transmission, %
1,00
0,96
0,92
0,88
0,84
-10
-8
-6
-4
-2
0
2
4
6
8
10
Velocity, mm/s

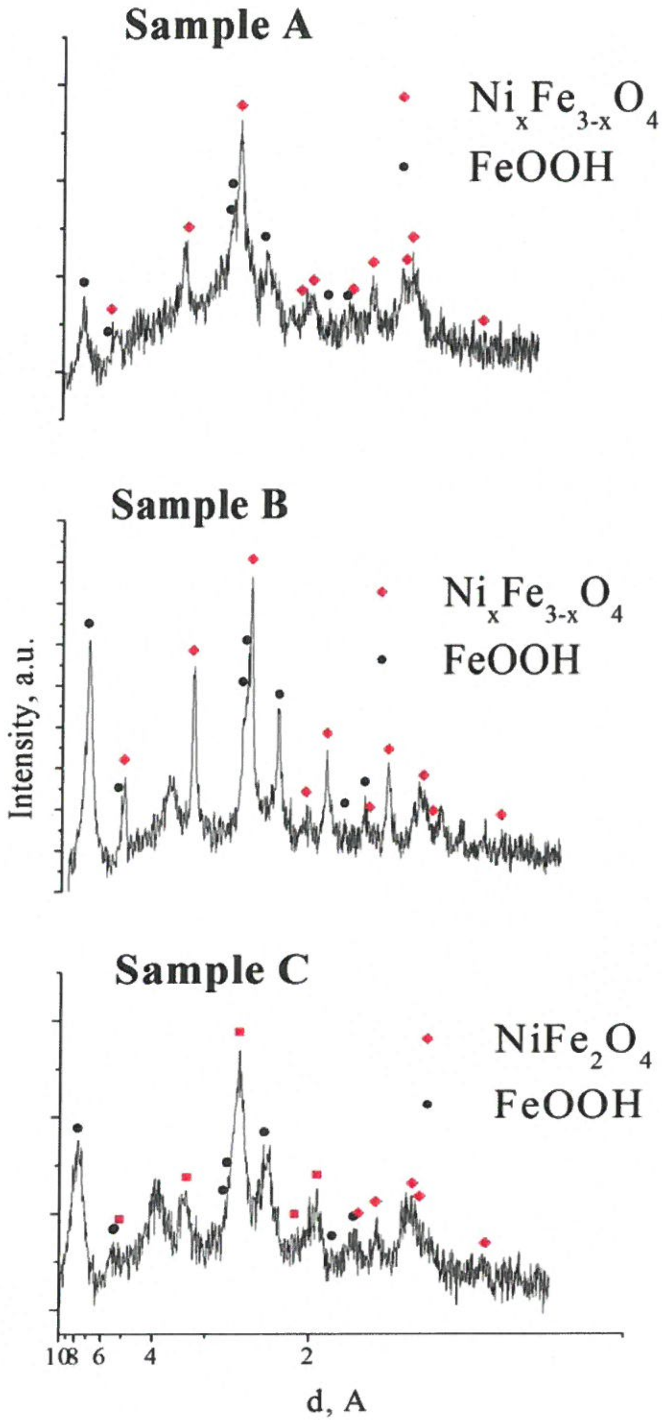

Sample A
$Ni_xFe_{3-x}O_4$
FeOOH
Sample B
$Ni_xFe_{3-x}O_4$
FeOOH
Intensity, a.u.
Sample C
$NiFe_2O_4$
FeOOH
10 8 6 4 2
d, A

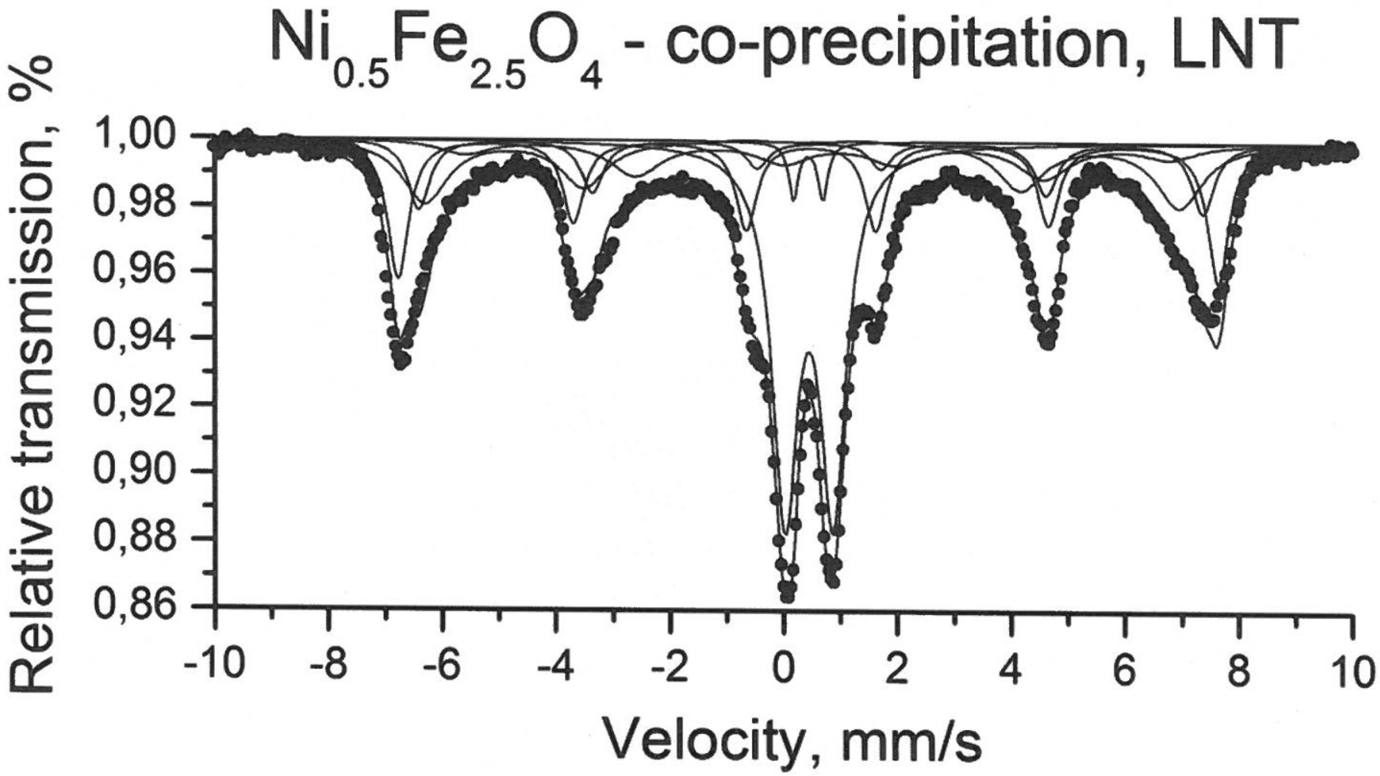
Ni0.5Fe2.5O4 - co-precipitation, LNT
Relative transmission, %
1,00
0,98
0,96
0,94
0,92
0,90
0,88
0,86
-10
-8
-6
-4
-2
0
2
4
6
8
10
Velocity, mm/s

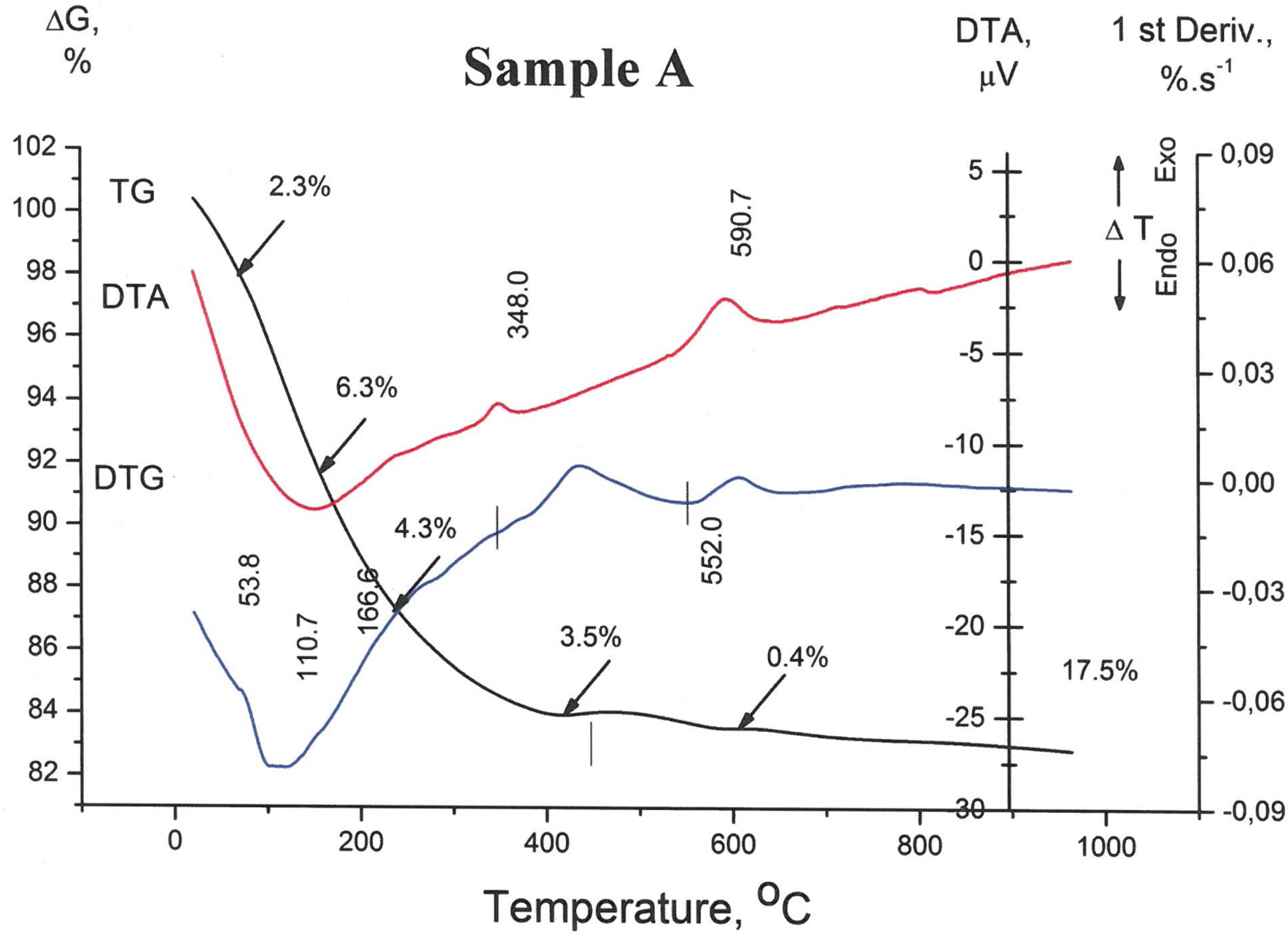

ΔG, %
Sample A
DTA, μV
1 st Deriv., %.s-1
102
100
98
96
94
92
90
88
86
84
82
TG
DTA
DTG
2.3%
6.3%
4.3%
3.5%
0.4%
17.5%
53.8
110.7
166.6
348.0
552.0
590.7
5
0
-5
-10
-15
-20
-25
-30
Exo
Δ T
Endo
0,09
0,06
0,03
0,00
-0,03
-0,06
-0,09
0
200
400
600
800
1000
Temperature, oC

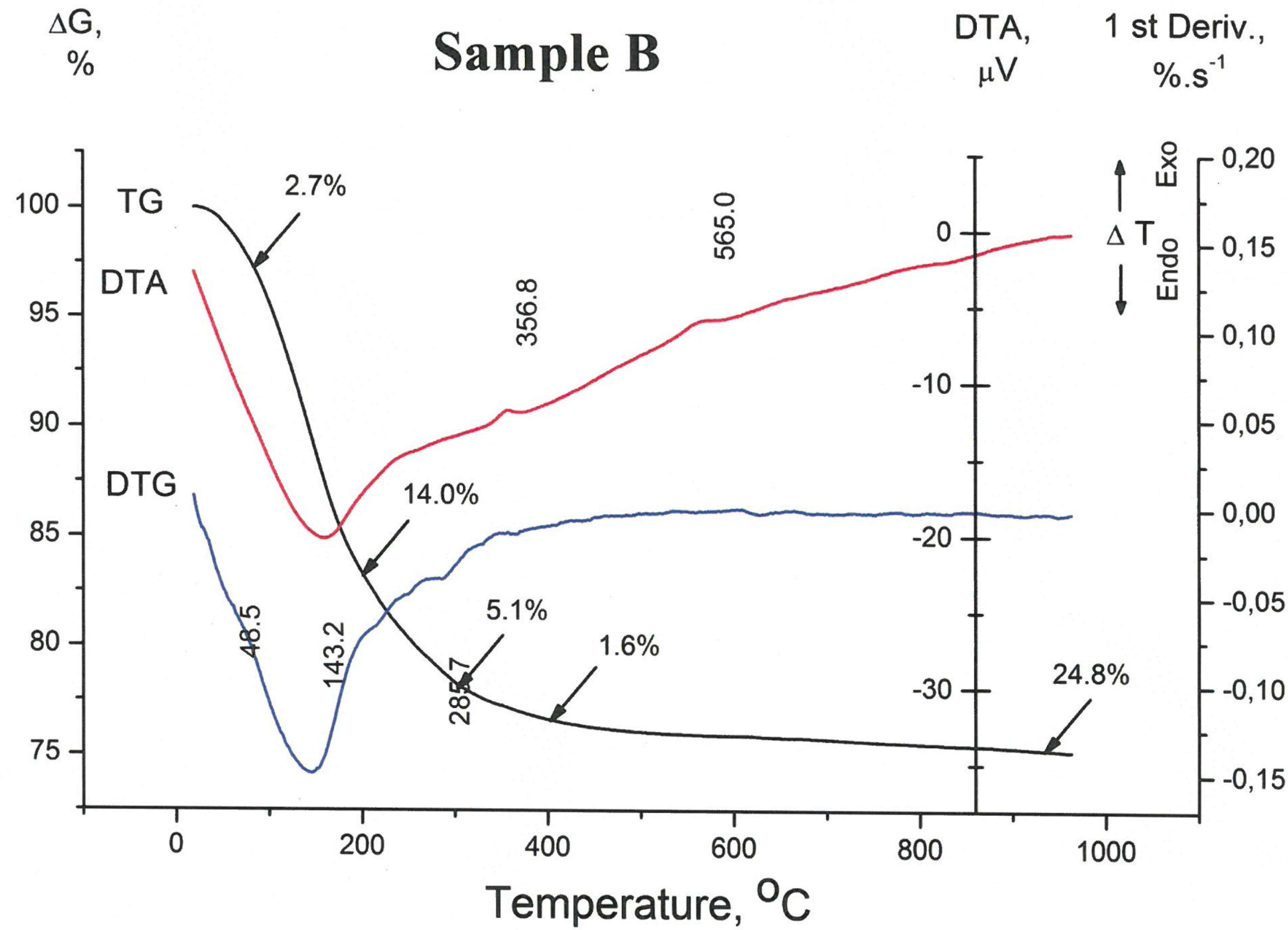
Sample B
ΔG,
%
DTA,
μV
1 st Deriv.,
%.s-1
TG
DTA
DTG
2.7%
14.0%
5.1%
1.6%
24.8%
48.5
143.2
285.7
356.8
565.0
Exo
Δ T
Endo
100
95
90
85
80
75
0
-10
-20
-30
0,20
0,15
0,10
0,05
0,00
-0,05
-0,10
-0,15
0
200
400
600
800
1000
Temperature, oC

Sample C

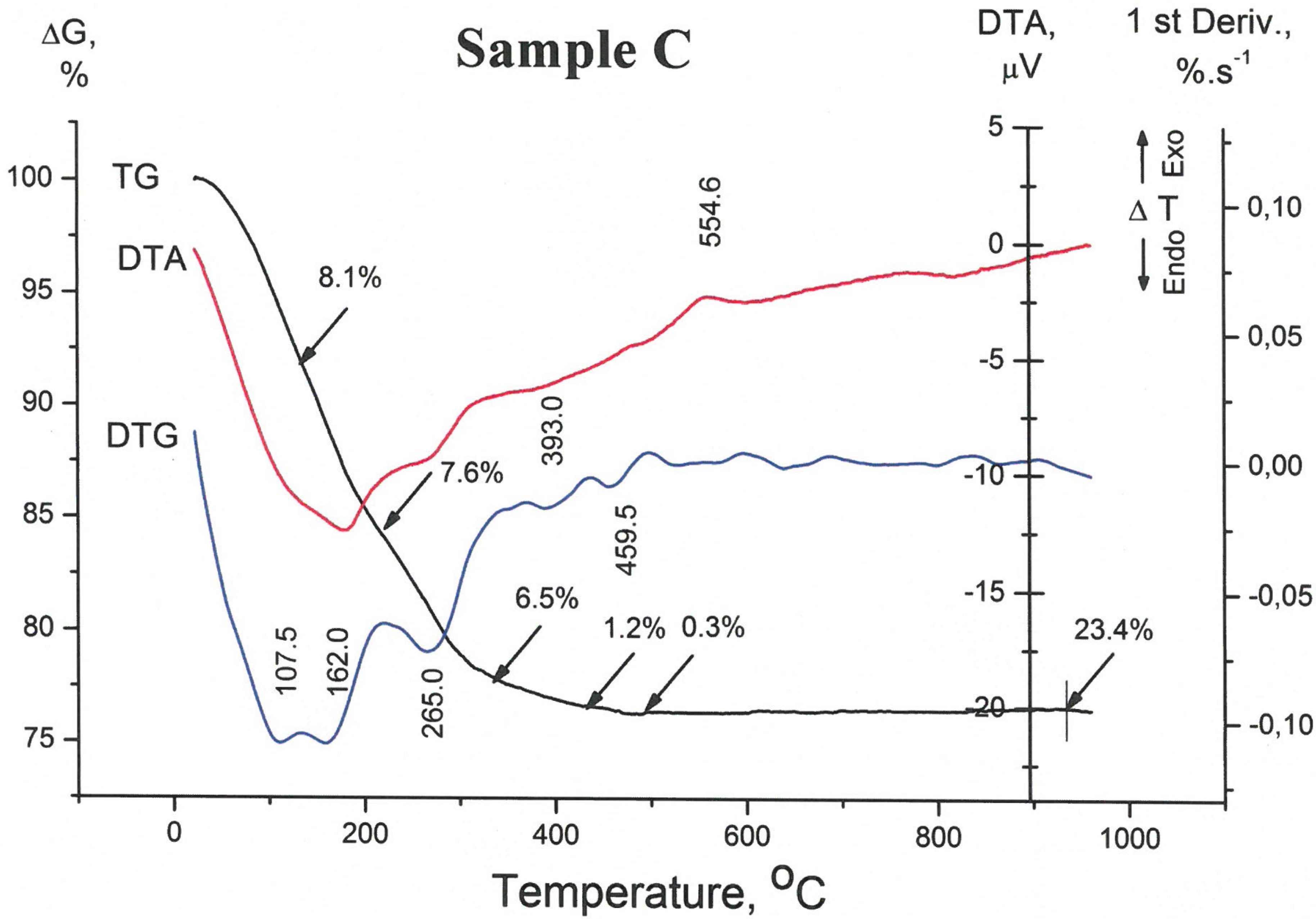

ΔG, %
DTA, μV
1 st Deriv., %.s-1
100
95
90
85
80
75
5
0
-5
-10
-15
-20
0,10
0,05
0,00
-0,05
-0,10
TG
DTA
DTG
8.1%
7.6%
6.5%
1.2%
0.3%
23.4%
107.5
162.0
265.0
393.0
459.5
554.6
Exo
Δ T
Endo
0
200
400
600
800
1000
Temperature, oC

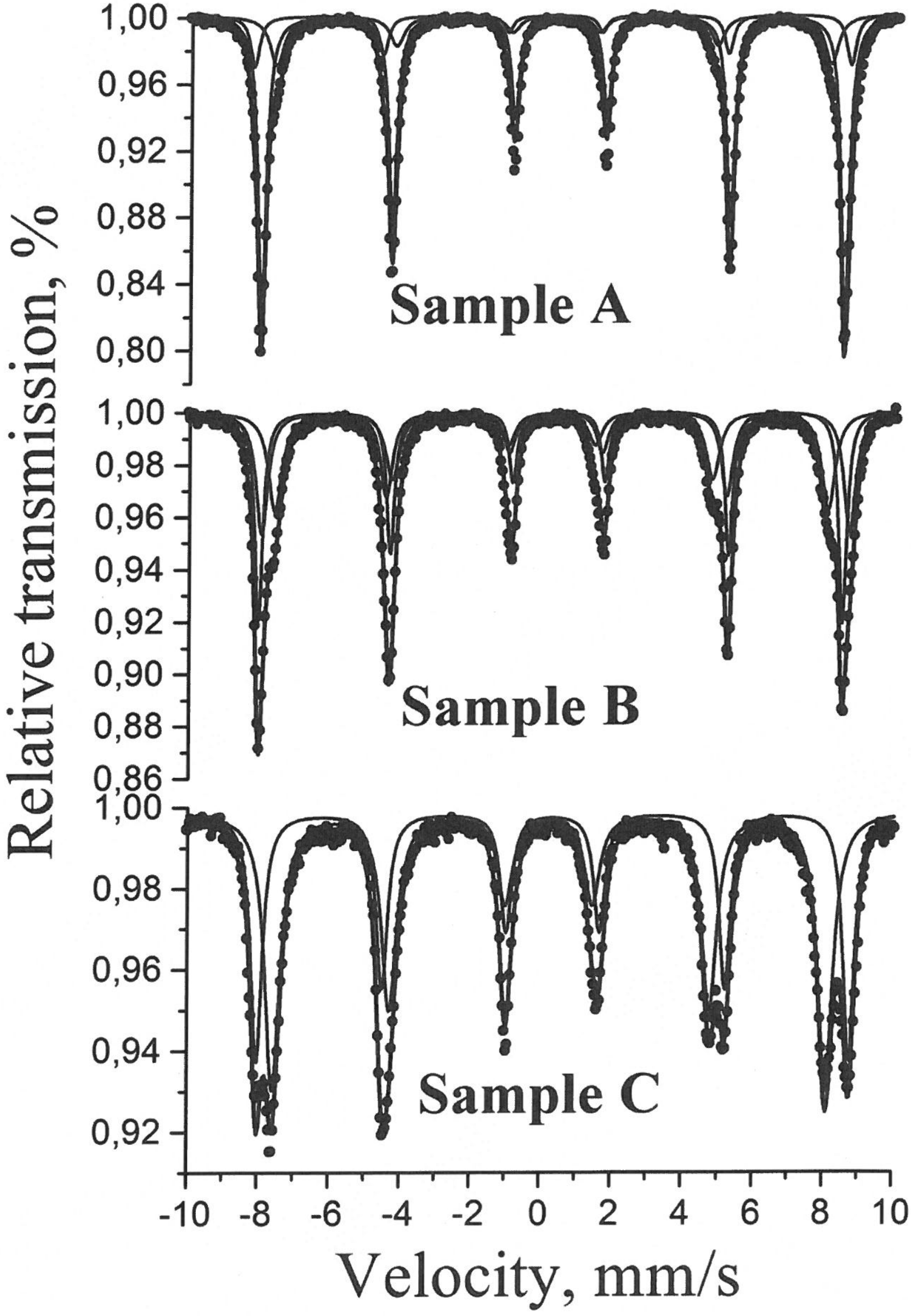

Relative transmission, %
Sample A
Sample B
Sample C
Velocity, mm/s
1,00
0,96
0,92
0,88
0,84
0,80
1,00
0,98
0,96
0,94
0,92
0,90
0,88
0,86
1,00
0,98
0,96
0,94
0,92
-10
-8
-6
-4
-2
0
2
4
6
8
10

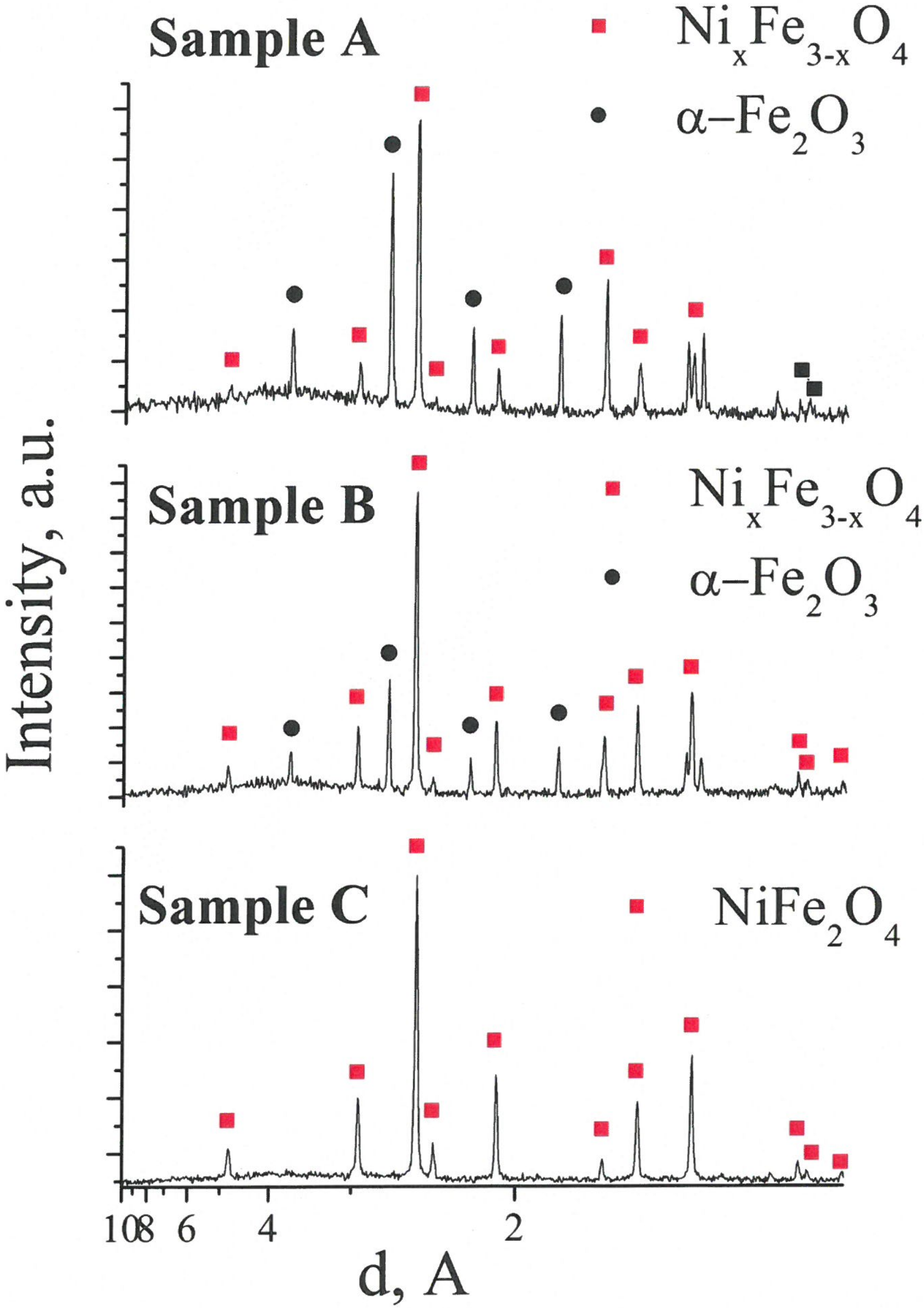

Sample A
$Ni_xFe_{3-x}O_4$
α–Fe_2O_3
Sample B
$Ni_xFe_{3-x}O_4$
α–Fe_2O_3
Sample C
$NiFe_2O_4$
Intensity, a.u.
10 8 6 4 2
d, A

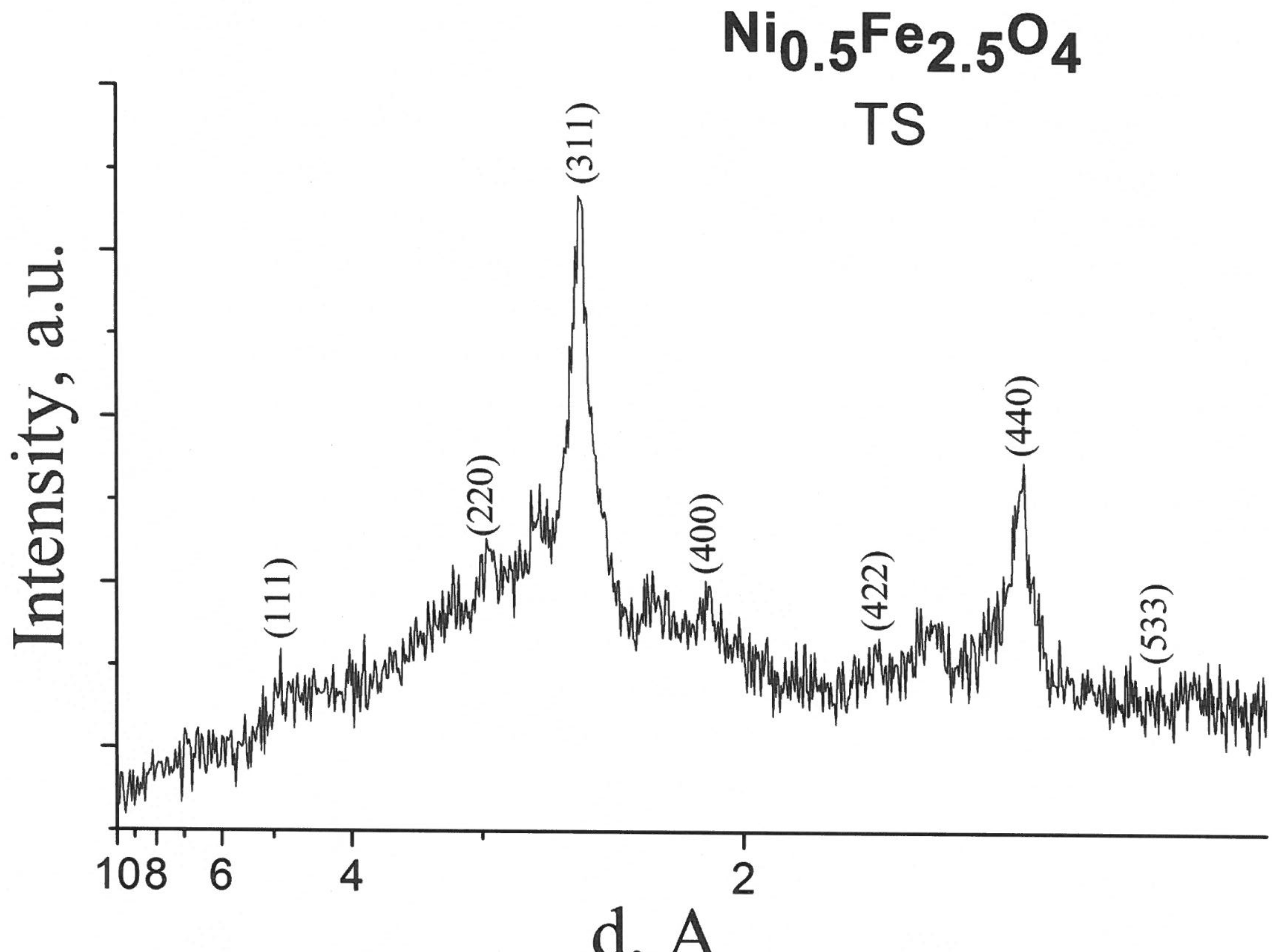

Ni0.5Fe2.5O4
TS
(111)
(220)
(311)
(400)
(422)
(440)
(533)
Intensity, a.u.
108
6
4
2
d, A

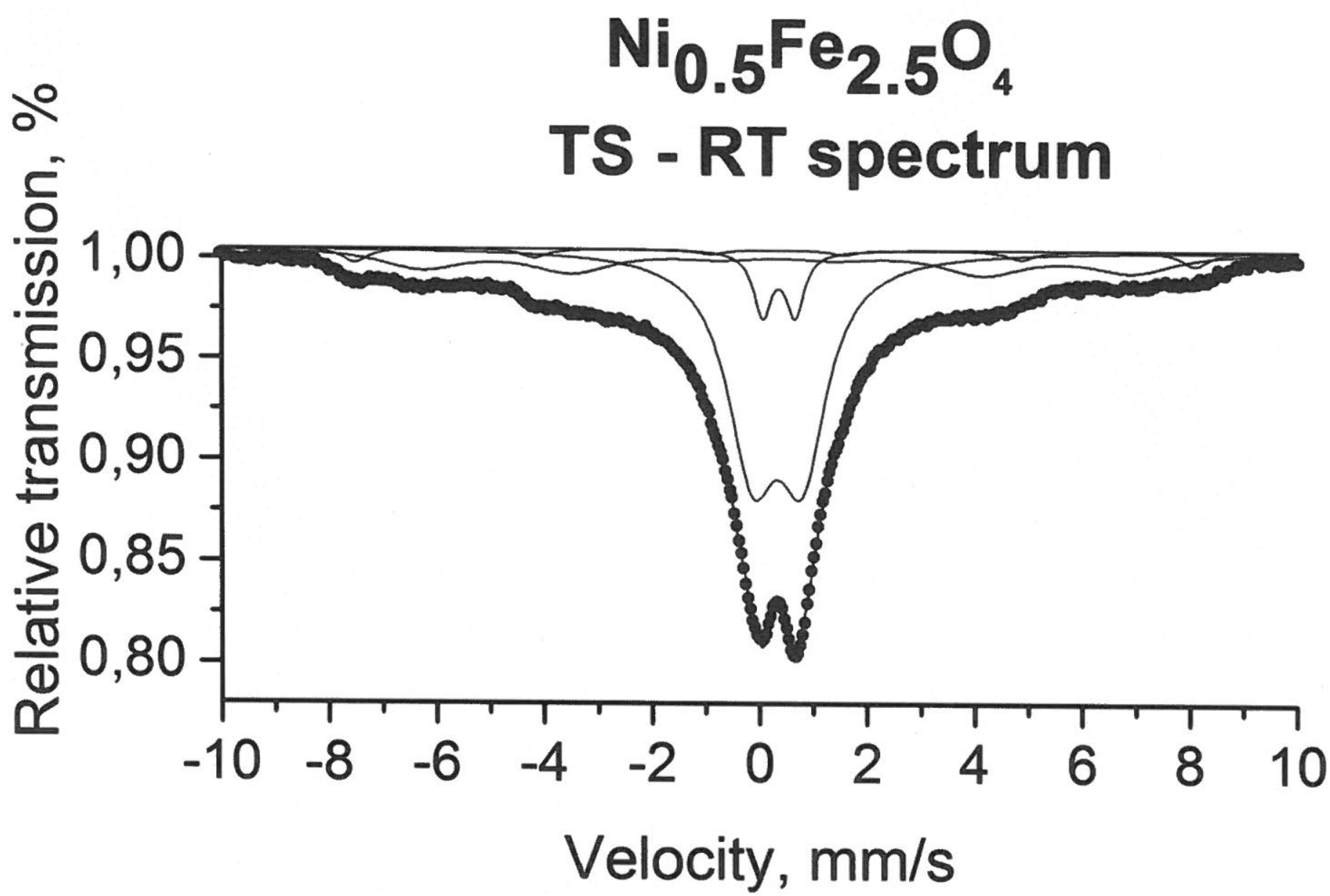

$Ni_{0.5}Fe_{2.5}O_4$
TS - RT spectrum
Relative transmission, %
1,00
0,95
0,90
0,85
0,80
-10 -8 -6 -4 -2 0 2 4 6 8 10
Velocity, mm/s

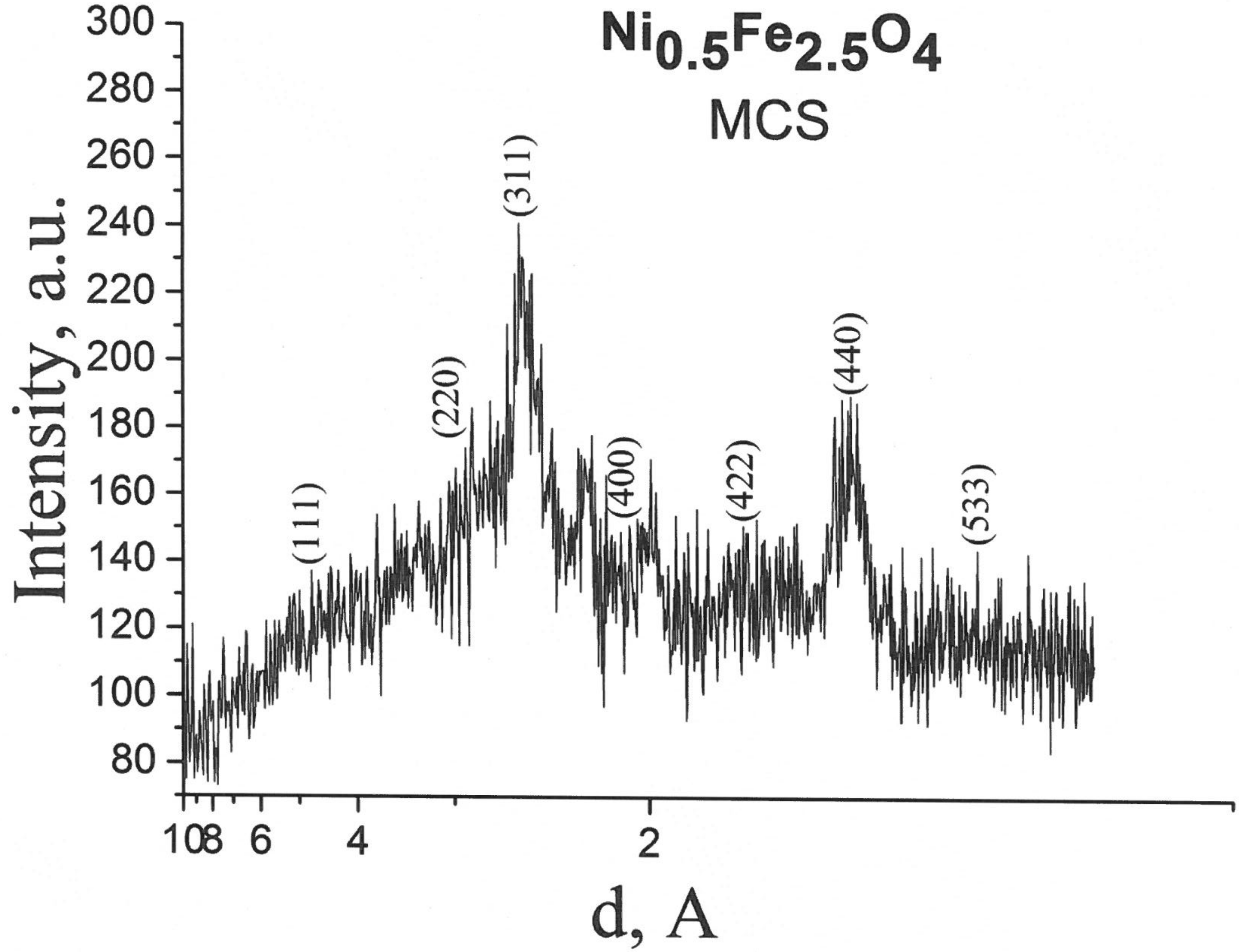

Ni0.5Fe2.5O4
MCS
Intensity, a.u.
300
280
260
240
220
200
180
160
140
120
100
80
(111)
(220)
(311)
(400)
(422)
(440)
(533)
10
8
6
4
2
d, A

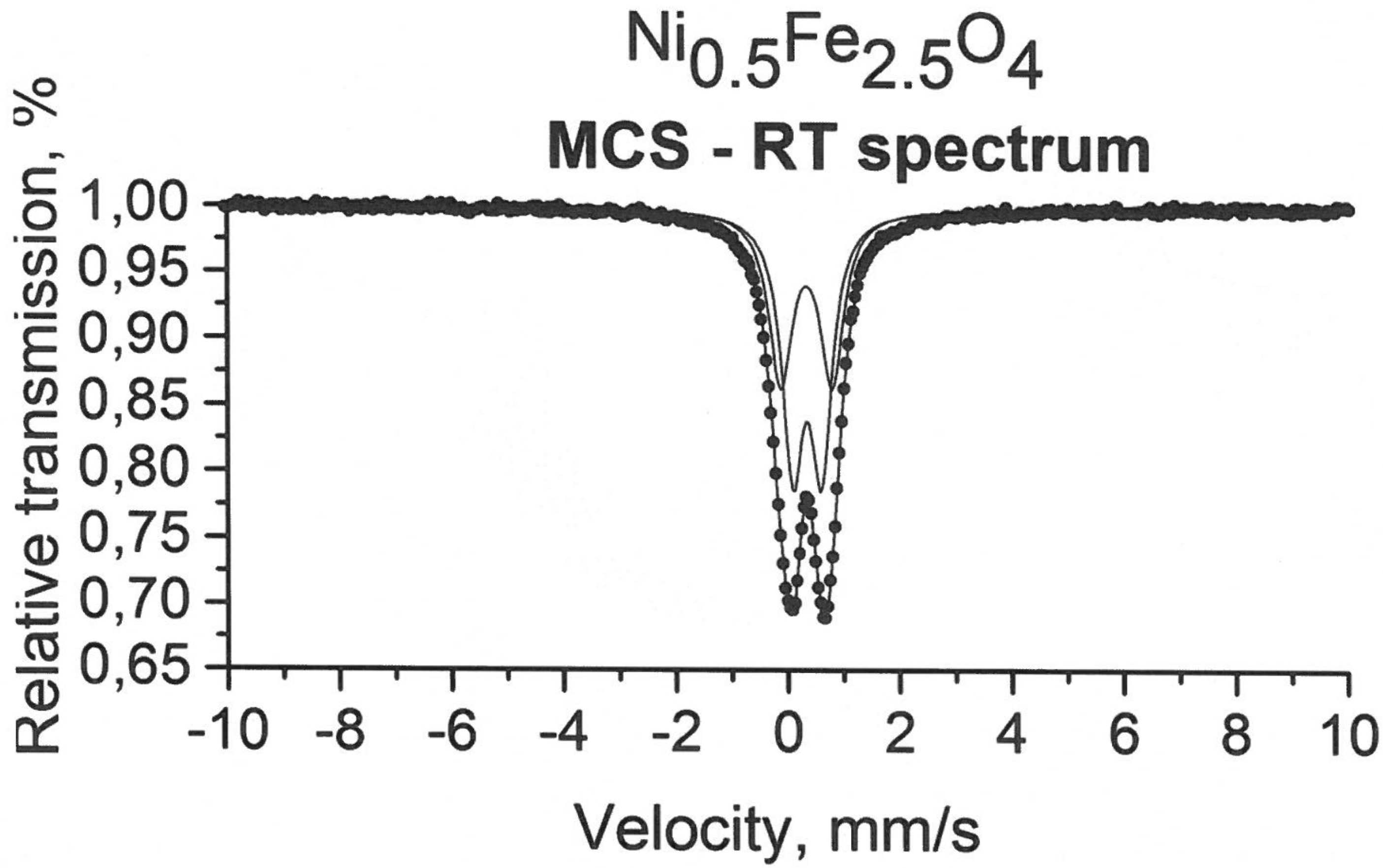
Ni0.5Fe2.5O4
MCS - RT spectrum
Relative transmission, %
1,00
0,95
0,90
0,85
0,80
0,75
0,70
0,65
-10
-8
-6
-4
-2
0
2
4
6
8
10
Velocity, mm/s

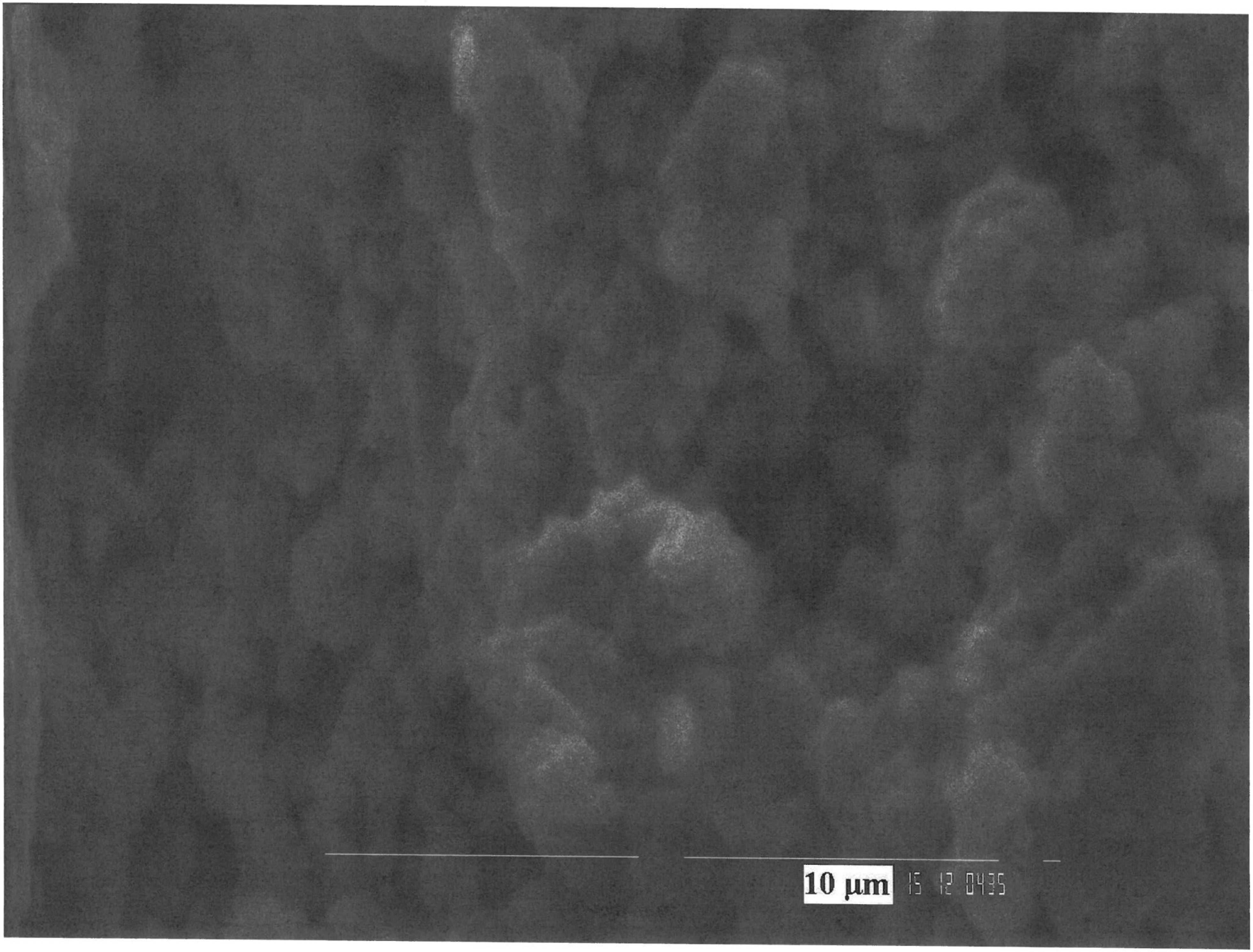
10 μm
15 12 0435

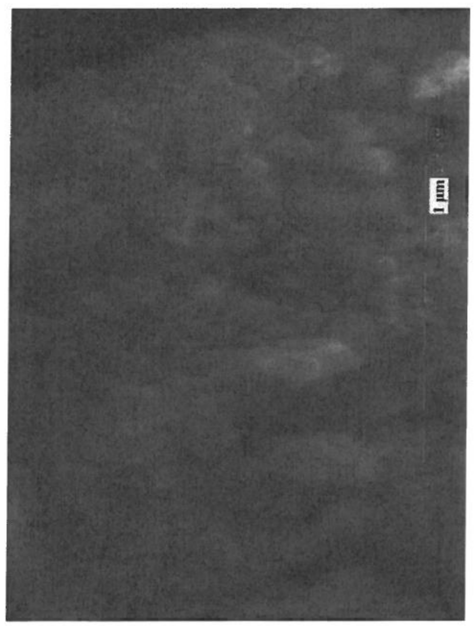
1 μm


10 µm

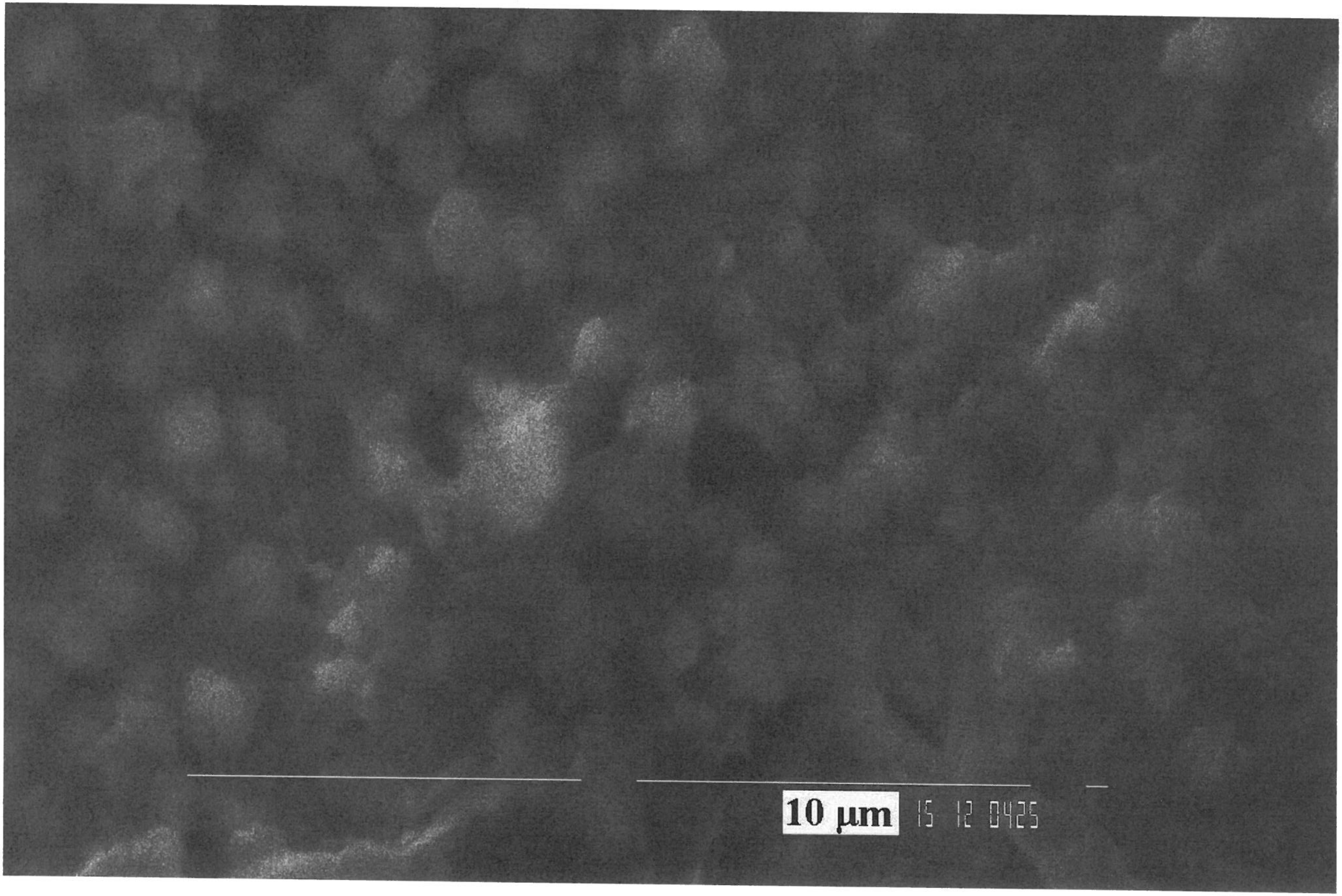
10 µm
15 12 0425

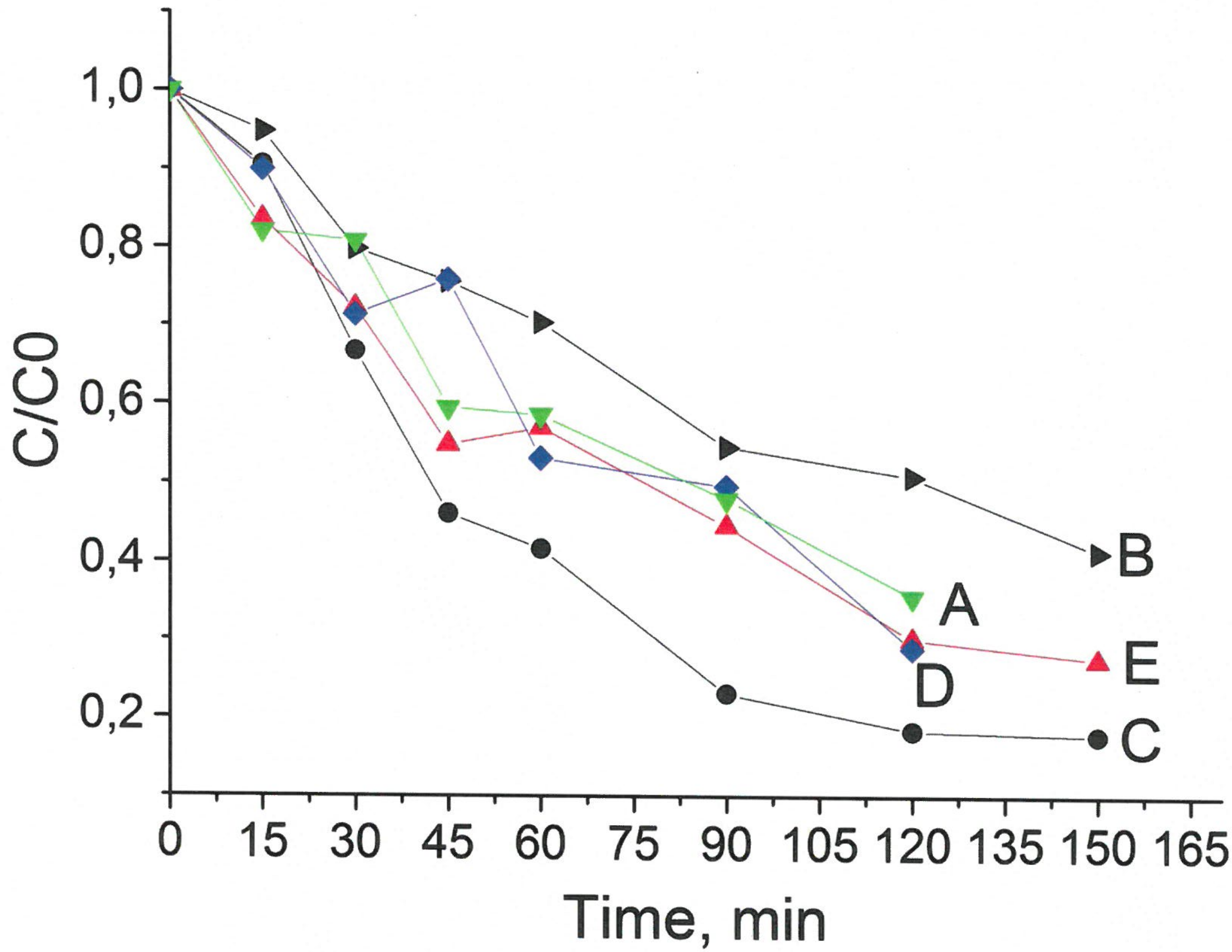
C/C0
1,0
0,8
0,6
0,4
0,2
0
15
30
45
60
75
90
105
120
135
150
165
Time, min
A
B
C
D
E